Hindawi
Advances in Materials Science and Engineering
Volume 2023, Article ID 2857678, 18 pages
https://doi.org/10.1155/2023/2857678

Research Article

Size-Dependent Thermoelastic Behavior Analysis of Functionally Graded Magneto-Electro-Elastic Cylindrical Shells Based on Modified Couple Stress Theory

Sajad Golchin Khazari, Younes Mohammadi, and Mohammad Mahdi Kheirikhah

Department of Mechanical Engineering, Qazvin Branch, Islamic Azad University, Qazvin, Iran

Correspondence should be addressed to Younes Mohammadi; u.mohammadi@qiau.ac.ir

Received 30 January 2022; Revised 8 November 2022; Accepted 8 December 2022; Published 30 April 2023

Academic Editor: Anish Maridhas

In this article, the influence of important parameters on the size-dependent thermoelastic behavior of functionally graded magneto-electro-thermo-elastic microcylinders (FGMEE) is studied by means of modified stress couple theory and under the influence of combined mechanical-thermal-magnetic loads. The equations of motion were derived by considering the linear behavior of the shells and considering the first-order theory of the nonlocal shear deformation of the shells. In the following, the results of solving the equations governing the buckle are analyzed. Based on this, firstly, the mechanical properties used in the shell are presented, then the linear buckling behavior is studied, and finally, the size-dependent buckling behavior of these structures is studied. In the presented results, the mode numbers of each buckling load are shown as n and m, where n and m represent the circumferential and longitudinal mode numbers, respectively. In the theory section, using the pairwise size-dependent theory, the stress is corrected, and considering the shell with a relatively thick geometric structure and the forces due to the heterogeneous thermal boundary conditions, a combination of convection heat transfer and displacement is used to obtain a three-dimensional shell temperature distribution. The equilibrium equations of the term electromagnetic coupling system are obtained using the first-order shear displacement field of the shell and the structural relationships in the functionally graded magneto-electro-thermo-elastic (FG-METE) intelligent material. Then, using appropriate analytical and numerical methods, various components of the displacement field, electrical and mechanical potential, and, most importantly, structural stresses for different boundary conditions are obtained.

1. Introduction

Smart materials today are widely used in advanced equipment and have become an exciting field of research. These materials display a predesigned behavior against external factors and are appropriate to the current situation. Some intelligent materials tend to get deformed by a change in the magnetic or electric field [1–5]. Many studies have been conducted on the applications of an essential group of intelligent composite materials in various industries, such as aerospace, automotive, and medical engineering. Also called intelligent materials, their mechanical and physical properties can change in different environmental conditions. A critical class of intelligent materials, magneto-electro-elastic (MEE) composite materials combine piezoelectric and piezomagnetic phases. In other words, they display a combination of piezoelectric and magneto-electric properties that these materials fail to provide independently [6–9]. Magneto-electro-elastic materials are very useful for intelligent applications, thanks to their ability to transfer energy in the electrical and mechanical magnetic phases. Piezomagnetic and piezoelectric materials can convert energy from one form to another, such as magnetic, electrical, mechanical, or thermal. Intelligent structures made of piezomagnetic and piezoelectric materials have magneto-electro-thermoplastics coupling effects [10–14]. This effect is not present in the piezomagnetic or piezoelectric material alone. Couplings between thermoplastics and electric fields

in piezoelectric materials allow sensing perturbations and thermomechanical disturbances from induced electrical and magnetic potential measurements [15–18]. Magneto-electro thermoplastic coupling effects have significant applications in sensors, capacitors, and vibration control devices. One of the basic elements for these intelligent structures is piezoelectric/piezomagnetic layered composite materials, which are generally subjected to mechanical and thermal loading. All states of energy, such as mechanical, electrical, magnetic, or metabolic, are eventually converted to thermal energy. Hence, thermal energy is one of the most present and available forms of energy. Unfortunately, a significant fraction of the available thermal energy is always converted into dissipative heat [19–22]. Vehicles, factories, power plants, electronic devices, and even the human body waste thousands of joules of thermal energy.

The utilization of dissipative thermal energy and its conversion into more useable forms, such as mechanical and thermal energy, has become a curious field of research in recent decades. Recently, the low-temperature thermal energy conversion mechanism has been based on the thermoelectric effect (TE). Thermoelectric transducers use a reflection effect when they have dissimilar hot ends of conductors at a connection point [1]. Thermoelectric heat exchangers have a relatively small heat conversion efficiency factor of 5% when the hot end is below 200°C, limiting their application and requiring a fundamentally different approach to converting heat energy into other useful forms of energy [23–25]. Thermomagnetic energy production is thermoelastic electro-magneto graded (TEMG). This method is based on the effect of heat on the magnetic properties of ferromagnetic materials that undergo a rapid phase change near the transfer temperature. The transfer temperature, also known as the blind temperature or blind spot, returns to a state in ferromagnetic material where the magnetizing property disappears, and the material is transferred to a paramagnetic state [26–29]. Very rapid changes in magnetization around a given temperature can be used to design a device that converts thermal energy into electrical energy, whether directly or indirectly with mechanical energy [30].

In this article, the influence of important parameters on the size-dependent thermoelastic behavior of functionally graded magneto-electro-thermo-elastic microcylinders (FGMEE) is studied by means of modified stress couple theory and under the influence of combined mechanical-thermal-magnetic loads. The equations of motion were derived by considering the linear behavior of the shells and the first-order theory of the nonlocal shear deformation of the shells. In the following, the results of solving the equations governing the buckling are analyzed. Based on this, firstly, the mechanical properties used in the shell are presented, then the linear buckling behavior is studied, and finally, the size-dependent buckle behavior of these structures is studied. In the presented results, the mode numbers of each buckling load are shown as n and m where n and m represent the circumferential and longitudinal mode numbers, respectively.

Akbarzadeh et al. [31] calculated the static response of the magneto-electro-elastic (MEE) sheet using finite element analysis. They showed that the sheet's vertical and transverse shear stresses could be studied as degrees of freedom by considering the mechanical deformation components and electrical and magnetic potentials. Using Lord-Schulman's theory to analyze the electro-magneto-thermoplastic response of thermoplastic magneto-electro-elastic (TMEE), a hollow cylinder made of magneto-electro-elastic (MEE) functionally graded material was used by Abbas and Zenkour [32] to study the effect of comfort time, temperature, and volume fraction of each phase on the static parameters of a smart-graded hollow cylinder. This study is presented as a guide for the Thermoelastic magneto-electro-elastic (TMEE) response of smart materials under the heat source influence.

Arefi [33] studied the static components of functionally graded magneto-electro-thermo-elastic (FG-METE) functionally graded beams, whose properties change exponentially with thickness and are subject to extensive spatial sinusoidal loading. Different results have been obtained for the exponential index parameters of the functionally scaled material for the electric potential and deformation curves. One of the advantages of smart materials with functionally graded magneto-electro-thermo-elastic (FG-METE) structures over smart materials with a layer structure is the absence of discontinuities in electrical displacement and magnetic induction between different layers of material. The static response of the functionally graded magneto-electro-thermo-elastic (FG-METE) stair coupling sheets under different thermal environmental conditions has been studied using finite element formulations. When subjected to no uniform temperature distribution, tensile stresses in the magneto astrictive phase of the material are induced in the joint-boundary boundary conditions. Boundary conditions also affect the magnetic and electrical potentials in the direction of displacement [34, 35]. The static behavior of the functionally graded magneto-electro-thermo-elastic (FG-METE) sheet receives dramatic effects from the uniform temperature distribution. The following effects tend to improve the static behavior of composites regardless of their temperature distribution profile. Studies on the effect of heat on multilayer magneto-electro-elastic (MEE) beams indicate the same behavior as functionally graded magneto-electro-thermo-elastic (FG-METE) stair sheets [36].

Kim and Baltazar [32] proposed a method to analyze some structural properties of multilayer composites made of functionally graded magneto-electro-thermo-elastic (FG-METE) material. Their analysis was based on matrix formulation for layered composite material coupling properties, including piezoelectricity, piezomagnetism, and thermoplastics. They finally obtained an analytical and closed-form solution for the effective properties of the smart functionally graded composite. They also numerically evaluated the effect of the gradient of the distributed function gradient on the pyro magnetic and pyroelectric constants. They showed that the effective pyroelectric and pyromagnetic constants for the composite intelligent graded material could significantly increase due to the distributed

gradient in the thickness about two times the original value. This constant variation is a function of the volume fraction of the different phases that make up the various layers of intelligent composite.

Sladek et al. [37] investigated the behavior of functionally graded magneto-electro-thermo-elastic (FG-METE) circular sheets using the meshless local Petrov–Galerkin (MLPG) method under articulated and trapped conditions. They concluded that the generated electric potential significantly affects the results of impact and static loads.

Arefi [33] introduced the linear coupling equations to study the electromechanical behavior of the shell with the desired shape and made of magneto-electro-elastic (MEE) functional graded material; these equations are further used for the analysis of cylindrical, spherical, and circular shells. They are fully functional, with the desired curvature and thickness.

Kattimani et al. [33] have conducted various studies on the static behavior of beams and intelligent composite sheets made of magneto-electro-elastic (MEE) electro-elastic magnetic materials placed in a thermal environment. A common feature of most of these papers is the used of linear coupling relationships in calculations and finite element analysis (FEA), and numerical solutions.

Wu and Lu [34] used a modified Pagano method to investigate the dynamic response of a functionally graded multilayer magneto-electro-elastic (MEE) sheet with a simple abutment under different surfaces conditions. They determined the conditions governing the surface for both free electric and magnetic potential states and free magnetic flux and electric flux and also used the exponential model to distribute the properties of the material in the thickness layer.

Phoenix et al. [35] proposed a layered model of magneto-electro-elastic (MEE) sheets and developed the Reisner mixed variational theorem to perform a static and dynamic analysis on magneto-electro-elastic (MEE) composite sheets.

Ootao and Ishihara [36] studied the analysis of hollow cylindrical shells of functionally graded magneto-electro-thermo-elastic (FG-METE) under uniform surface heating. They also studied the transient thermal stress problem for the above cylindrical shell considering the plane strain model and the effect of different parameters, such as inhomogeneity of materials and electrical and magnetic potentials on thermal stress.

Huang et al. [38] developed analytical and semi-analytical models to change static parameters in the direction of beam thickness. For the problem of general two-dimensional stress, they assumed the functions governing stress, electrical displacement, and magnetic induction in two main parts, the first part as a trigonometric function in the longitudinal dimension and the axial direction of the beam and the second part as an unknown function in the thickness direction. They presented their analysis for different boundary conditions.

2. Relationships and Equations

2.1. Mathematical Model and Governing Formulation. Figure 1 shows a schematic of the problem model, which is a relatively thick cylindrical shell located in an electromagnetic field [12]. The electric field and the magnetic field are included in the problem. The microshell's radius, thickness, and length are also displayed with R, h, and L, respectively.

According to the first-order shear deformation theory of shells, the displacement field of a cylindrical shell in three different directions of the cylindrical coordinate system x, θ, z is shown by the following equation [8–10]:

$$\begin{aligned} u(x,\theta,z,t) &= u_0(x,\theta,t) + z\psi_x(x,\theta,t),\\ v(x,\theta,z,t) &= v_0(x,\theta,t) + z\psi_\theta(x,\theta,t),\\ w(x,\theta,z,t) &= w_0(x,\theta,t), \end{aligned} \tag{1}$$

where $u\_0\ (x, \theta, t)$, $v\_0\ (x, \theta, t)$, and $w\_0\ (x, \theta, t)$ represent axial, peripheral, and radial deformations. Also, $\psi\_x\ (x, \theta, t)$ and $\psi\_\theta\ (x, \theta, t)$ represent the rotation of the vector perpendicular to an element in the middle plate of the sheet thickness in the circumferential and axial directions. The kinematic relationships for a linear isotropic elastic material can be expressed by considering and applying components related to the kinematic parameters that affect the strain energy. Nonetheless, strain tensors in the material are as follows [13–15]:

$$\begin{aligned} \varepsilon_{ij} &= \frac{1}{2}\left(u_{i,j} + u_{j,i}\right),\\ \chi^s_{ij} &= \frac{1}{2}\left(\varphi_{i,j} + \varphi_{j,i}\right),\\ m^s_{ij} &= 2l^2\mu\chi^s_{ij},\\ \theta_i &= \frac{1}{2}\left(curl\,(u)\right). \end{aligned} \tag{2}$$

In the above equations, $m^s{}_{ij}\ \hat{}$ expresses high-order stresses. Also, ε_{ij}, $X^s{}_{ij}$ represent the strain tensor and the expansion gradient. In addition, u_i and φ_i also represent minimal displacement vector components, respectively. On the other hand, the strain components in the shell are as follows [17]:

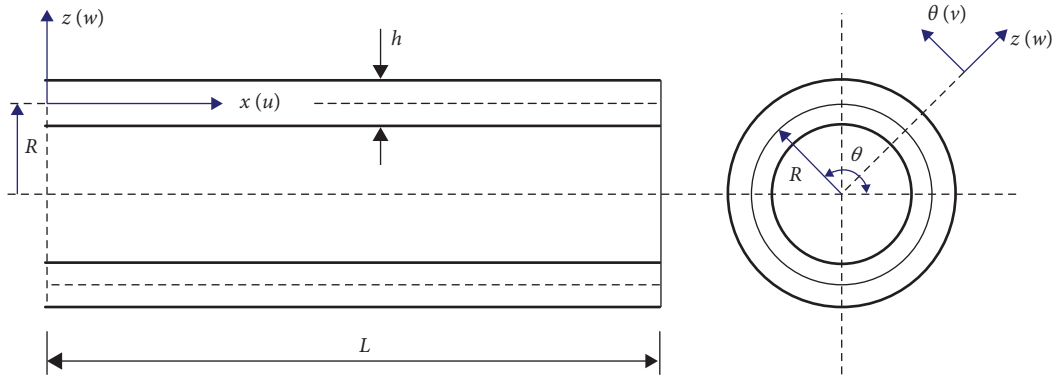

Figure 1: Schematic of a functionally graded magneto-electro-elastic cylindrical shell with arbitrary boundary conditions at both ends.

$$\begin{aligned}
\varepsilon_{xx} &= \frac{\partial u}{\partial x} + z\frac{\partial \psi_x}{\partial x},\\
\varepsilon_{\theta\theta} &= \frac{1}{R}\frac{\partial v}{\partial \theta} + z\frac{1}{R}\frac{\partial \psi_\theta}{\partial \theta} + \frac{w}{R},\\
\varepsilon_{xz} &= \frac{1}{2}\left(\psi_x + \frac{\partial w}{\partial x}\right),\\
\varepsilon_{x\theta} &= \frac{1}{2}\left(\frac{1}{R}\frac{\partial u}{\partial \theta} + \frac{\partial v}{\partial x}\right) + \frac{z}{2}\left(\frac{1}{R}\frac{\partial \psi_x}{\partial \theta} + \frac{\partial \psi_\theta}{\partial x}\right),\\
\varepsilon_{\theta z} &= \frac{1}{2}\left(\psi_\theta + \frac{1}{R}\frac{\partial w}{\partial \theta} - \frac{v}{R}\right).
\end{aligned} \tag{3}$$

The nonzero components of the symmetric rotational gradient tensor are as follows [19]:

$$\begin{aligned}
\chi^s_{xx} &= -\frac{1}{2}\left(\frac{\partial \psi_\theta}{\partial x} + \frac{1}{R}\frac{\partial v}{\partial x} - \frac{1}{R}\frac{\partial^2 w}{\partial x \partial \theta}\right),\\
\chi^s_{\theta\theta} &= -\frac{1}{2R}\left(\frac{1}{R}\frac{\partial u}{\partial \theta} - \frac{\partial v}{\partial x} - z\frac{\partial \psi_\theta}{\partial x}\right) - \frac{1}{2}\left(\frac{1}{R}\frac{\partial^2 w}{\partial x \partial \theta} - \frac{1}{R}\frac{\partial \psi_x}{\partial \theta}\right),\\
\chi^s_{zz} &= -\frac{1}{2}\left(\frac{1}{R}\frac{\partial \psi_x}{\partial \theta} - \frac{\partial \psi_\theta}{\partial x} - \frac{1}{R^2}\frac{\partial u}{\partial \theta}\right),\\
\chi^s_{x\theta} &= -\frac{1}{4}\left(\frac{1}{R^2}\frac{\partial v}{\partial \theta} + \frac{\partial^2 w}{\partial x^2} - \frac{1}{R^2}\frac{\partial^2 w}{\partial \theta^2} - \frac{\partial \psi_x}{\partial x} + \frac{1}{R}\frac{\partial \psi_\theta}{\partial \theta}\right),\\
\chi^s_{xz} &= -\frac{1}{4}\left(\frac{1}{R}\frac{\partial^2 u}{\partial x \partial \theta} - \frac{\partial^2 v}{\partial x^2} - \frac{v}{R^2} + \frac{1}{R^2}\frac{\partial w}{\partial \theta} + \frac{\psi_\theta}{R}\right) - \frac{z}{4}\left(\frac{1}{R}\frac{\partial^2 \psi_\theta}{\partial x \partial \theta} - \frac{\partial^2 \psi_\theta}{\partial x^2}\right),\\
\chi^s_{\theta z} &= -\frac{1}{4}\left(\frac{1}{R^2}\frac{\partial^2 u}{\partial \theta^2} - \frac{1}{R}\frac{\partial^2 v}{\partial x \partial \theta} - \frac{1}{R}\frac{\partial w}{\partial x} + \frac{\psi_x}{R}\right) - \frac{z}{4}\left(\frac{1}{R^2}\frac{\partial^2 \psi_x}{\partial \theta^2} - \frac{1}{R}\frac{\partial^2 \psi_\theta}{\partial x \partial \theta}\right).
\end{aligned} \tag{4}$$

This paper investigates the properties of the cylindrical shell material of graded magneto-electro-elastic materials as a function that varies continuously and in the radial direction of the z-axis based on the exponential model of the graded material. Therefore, each property of the substance can be expressed as follows [20]:

$$P(z) = P_o V_c(z) + P_i V_m(z), \tag{5}$$

where P_o and P_i express the properties of the outer and inner shell surfaces. These surfaces are assumed to be all-ceramic and all-metal, respectively. Besides, the relationship between the volume fraction of the two smart phases of the smart functionally graded magneto is [21]:

$$V_{BaTiO3}(z) + V_{CoFe2O4}(z) = 1. \tag{6}$$

Based on the combination law and the relations [22]:

$$\begin{aligned} P(z) &= (P_o - P_i)V_c(z) + P_i, \\ V_{CoFe2O4}(z) &= \left(0.5 + \frac{z}{h}\right)^n. \end{aligned} \tag{7}$$

In the abovementioned relation, n is the exponential index of the smart two-phase functionally graded magneto, whose different properties can be expressed as follows [23]:

$$\begin{aligned} C_{ij}(z) &= \left(\left(C_{ijc} - C_{ijm}\right)\left(\frac{1}{2} + \frac{z}{h}\right)^n + C_{ijm}\right), \\ \rho(z) &= \left(\left(\rho_c - \rho_m\right)\left(\frac{1}{2} + \frac{z}{h}\right)^n + \rho_m\right), \\ \nu(z) &= \left(\left(\nu_c - \nu_m\right)\left(\frac{1}{2} + \frac{z}{h}\right)^n + \nu_m\right), \\ q_{ij}(z) &= \left(\left(q_{ijc} - q_{ijm}\right)\left(\frac{1}{2} + \frac{z}{h}\right)^n + q_{ijm}\right), \\ \chi_{ij}(z) &= \left(\left(\chi_{ijc} - \chi_{ijm}\right)\left(\frac{1}{2} + \frac{z}{h}\right)^n + \chi_{ijm}\right). \end{aligned} \tag{8}$$

The following are the structural relationships for a magneto-electro-elastic multiphase material with a functionally graded structure in terms of thickness in the thermal environment and with electrical and magnetic potential [24]:

$$\begin{aligned} \begin{bmatrix} \sigma_{xx} \\ \sigma_{\theta\theta} \\ \tau_{x\theta} \\ \tau_{\theta z} \\ \tau_{xz} \end{bmatrix} &= [c(z)] \begin{bmatrix} \varepsilon_{xx} \\ \varepsilon_{\theta\theta} \\ \gamma_{x\theta} \\ \gamma_{\theta z} \\ \gamma_{xz} \end{bmatrix} - [e(z)] \begin{bmatrix} E_x \\ E_\theta \\ E_z \end{bmatrix} - [q(z)] \begin{bmatrix} H_x \\ H_\theta \\ H_z \end{bmatrix} - \{\beta(z)\}\Delta T, \\ \begin{bmatrix} D_x \\ D_\theta \\ D_z \end{bmatrix} &= [e(z)]^T \begin{bmatrix} \varepsilon_{xx} \\ \varepsilon_{\theta\theta} \\ \gamma_{x\theta} \\ \gamma_{\theta z} \\ \gamma_{xz} \end{bmatrix} + [s(z)] \begin{bmatrix} E_x \\ E_\theta \\ E_z \end{bmatrix} + [d(z)] \begin{bmatrix} H_x \\ H_\theta \\ H_z \end{bmatrix} + \{p(z)\}\Delta T, \\ \begin{bmatrix} B_x \\ B_\theta \\ B_z \end{bmatrix} &= [q(z)]^T \begin{bmatrix} \varepsilon_{xx} \\ \varepsilon_{\theta\theta} \\ \gamma_{x\theta} \\ \gamma_{\theta z} \\ \gamma_{xz} \end{bmatrix} + [d(z)] \begin{bmatrix} E_x \\ E_\theta \\ E_z \end{bmatrix} + [r(z)] \begin{bmatrix} H_x \\ H_\theta \\ H_z \end{bmatrix} + \{\lambda(z)\}\Delta T. \end{aligned} \tag{9}$$

On the other hand, in equation (9), we have a magneto-electro-thermo-elastic smart functionally graded magneto [25]:

$$
\begin{aligned}
[c(z)] &= \begin{bmatrix} c_{11}(z) & c_{12}(z) & 0 & 0 & 0 \\ c_{12}(z) & c_{22}(z) & 0 & 0 & 0 \\ 0 & 0 & c_{66}(z) & 0 & 0 \\ 0 & 0 & 0 & c_{55}(z) & 0 \\ 0 & 0 & 0 & 0 & c_{44}(z) \end{bmatrix}, \\
[e(z)] &= \begin{bmatrix} 0 & 0 & e_{31}(z) \\ 0 & 0 & e_{32}(z) \\ 0 & 0 & 0 \\ 0 & e_{24}(z) & 0 \\ e_{25}(z) & 0 & 0 \end{bmatrix}, \\
[q(z)] &= \begin{bmatrix} 0 & 0 & q_{31}(z) \\ 0 & 0 & q_{32}(z) \\ 0 & 0 & 0 \\ 0 & q_{24}(z) & 0 \\ q_{25}(z) & 0 & 0 \end{bmatrix}, \\
[s(z)] &= \begin{bmatrix} s_{11}(z) & 0 & 0 \\ 0 & s_{22}(z) & 0 \\ 0 & 0 & s_{22}(z) \end{bmatrix}, \\
[d(z)] &= \begin{bmatrix} d_{11}(z) & 0 & 0 \\ 0 & d_{22}(z) & 0 \\ 0 & 0 & d_{33}(z) \end{bmatrix}, \\
[r(z)] &= \begin{bmatrix} r_{11}(z) & 0 & 0 \\ 0 & r_{22}(z) & 0 \\ 0 & 0 & r(z) \end{bmatrix}, \\
\{p(z)\} &= \begin{Bmatrix} p_1(z) \\ p_2(z) \\ p_3(z) \end{Bmatrix}, \\
\{\lambda(z)\} &= \begin{Bmatrix} \lambda_1(z) \\ \lambda_2(z) \\ \lambda_3(z) \end{Bmatrix}.
\end{aligned}
\tag{10}
$$

In order to satisfy Maxwell's quasistatic relations, the electric and magnetic fields are considered negative gradients of electric potentials $\tilde{\Phi}(x, \theta, z, t)$ and magnetic $\Psi(x, \theta, z, t)$:

$$
\begin{aligned}
E_x &= -\frac{\partial \tilde{\Phi}}{\partial x}, \\
E_\theta &= -\frac{1}{R+z}\frac{\partial \tilde{\Phi}}{\partial \theta}, \\
E_z &= -\frac{\partial \tilde{\Phi}}{\partial z}, \\
H_x &= -\frac{\partial \tilde{\Psi}}{\partial x}, \\
H_\theta &= -\frac{1}{R+z}\frac{\partial \tilde{\Psi}}{\partial \theta}, \\
H_z &= -\frac{\partial \tilde{\Psi}}{\partial z}.
\end{aligned}
\tag{11}
$$

The boundary conditions of the electric and magnetic fields at the upper and lower levels of the cylindrical shell are as follows:

$$
\begin{aligned}
\tilde{\Phi}\left(x, y, -\frac{h}{2}, t\right) &= -\phi_0, \\
\tilde{\Phi}\left(x, y, \frac{h}{2}, t\right) &= \phi_0, \\
\tilde{\Psi}\left(x, y, -\frac{h}{2}, t\right) &= -\Psi_0, \\
\tilde{\Psi}\left(x, y, \frac{h}{2}, t\right) &= \Psi_0,
\end{aligned}
\tag{12}
$$

where ϕ_0 and Ψ_0 are external electrical potentials and external magnetic potentials. According to the magnetic-electric boundary conditions, the explicit distribution of electrical and magnetic potentials is presented as a combination of linear and cosine changes in the following form [26].

$$
\begin{aligned}
\Phi(x, y, z, t) &= -\cos\left(\frac{\pi z}{h}\right)\phi(x, y, t) + \frac{2z\phi_0}{h}, \\
\Psi(x, y, z, t) &= -\cos\left(\frac{\pi z}{h}\right)\psi(x, y, t) + \frac{2z\psi_0}{h},
\end{aligned}
\tag{13}
$$

here $\phi(x, y, t)$ and $\psi(x, y, t)$ are spatial variations related to electrical and magnetic potentials in the x and θ directions.

3. Results and Discussion

3.1. Introduction. In this article, the influence of important parameters on the size-dependent thermoelastic behavior of functionally graded magneto-electro-thermoelastic microcylinders (FGMEE) is studied by means of modified stress couple theory and under the influence of combined mechanical-thermal-magnetic loads. The equations of motion were derived by considering the linear behavior of the shells and the first-order theory of the non-local shear deformation of the shells. In the following, the results of solving the equations governing the buckle are analyzed. Based on this, firstly, the mechanical properties used in the shell are presented, then the linear buckling behavior is studied, and finally, the size-dependent buckling behavior of these structures is studied. In the presented results, the mode numbers of each buckling load are shown as where n and m represent the circumferential and longitudinal mode numbers, respectively. Also, considering that the effect of different boundary conditions is also investigated for the sake of brevity, the simple, free, and clamped boundary conditions are named with the letters *S*, *F*, and *C*, respectively, thus the boundary conditions of simple supports at both ends, two headed head, free head-head, and simple head-head are denoted by the symbols SS, CC, CF, and CS. It should be noted that in all cases, the shear correction factor has been used. Also, the FGMEE microshell material used in the analyzes is the two-phase $BaTiO_3$-$CoFe_2O_4$ material due to its unique properties such as good mechanical properties, high chemical stability, and suitability for various heat processes, whose mechanical characteristics are given in Table 1. The intended FGMEE microshell consists of two piezoelectric phases of barium titanate ($BaTiO_3$) or phase B and piezomagnetic phase of cobalt ferrite ($CoFe_2O_4$) or phase C, so that the material properties gradually change along the thickness and from the inner surface to the outer surface, i.e., the surface The exterior of the cylindrical shell is rich in piezoelectric material, and the inner surface of the shell is rich in piezomagnetic material. Barium titanate is a ferroelectric ceramic material that exhibits the effects of light refraction and piezoelectric properties, which is used in capacitors, electromechanical transducers, and optics. Also, cobalt ferrite is a hard magnetic material with an inverse spinel structure, which is due to its unique properties compared to other ferrites, such as magnetic anisotropy, balanced saturation magnetization (MS), high coercive force (HC), mechanical hardness, and high chemical stability. Special attention has been paid to it and it is used as one of the important compounds in magnetic recording environments because the high magnetic coercive force is the main factor in increasing the volume of magnetic storage.

The changes of the modulus of elasticity against the thickness obtained from the power changes in the power law relationship for FGM composed of $BaTiO_3$ and $CoFe_2O_4$ are shown in Figure 2. As can be seen, the and states represent the isotropic shells made of $CoFe_2O_4$ and $BaTiO_3$, respectively.

Table 1: Mechanical properties of materials used in a two-phase $BaTiO_3$-$CoFe_2O_4$ FGMEE microshell [1].

Mechanical properties	$BaTiO_3$	$CoFe_2O_4$
C11 (GPa)	166	286
C12 (GPa)	77	173
C13 (GPa)	78	170
C33 (GPa)	162	269.5
C44 (GPa)	43	45.3
C66 (GPa)	44.5	56.5
e15 (C/m^2)	11.6	0
e31 (C/m^2)	−4.4	0
e33 (C/m^2)	18.6	0
s11 (10^{-9} C/Vm)	11.2	0.08
s33 (10^{-9} C/Vm)	12.6	0.093
q15 (N/Am)	0	550
q31 (N/Am)	0	580.3
q33 (N/Am)	0	699.7
d11 (Ns2/VC)	0	0
d33 (Ns2/VC)	0	0

In addition, in presenting the results, dimensionless critical loads are used, which are defined as follows:

$$\rho_{cr} = \frac{P_{cr}}{P_{cl}}, \tag{14}$$

where it is the critical load obtained by solving the equations and represents the critical buckling load for the classical shell, which is as follows for the cylindrical shell with simple boundary conditions [2]:

$$P_{cl} = \frac{2\pi h^2}{R^2\sqrt{3\left(1-\nu^2\right)}}. \tag{15}$$

3.2. Verification of Results. In the following, four comparative studies have been conducted between the results of the present project and the existing articles. In order to ensure the correctness and accuracy of the obtained answers, at first a comparison was made between the critical temperature difference of the cylindrical shell presented in reference [3] and the value obtained in this research; the results are listed in Table 2. It can be seen that the difference in the obtained results is appropriate and expected, and it can be accepted considering the percentage of differences between the results obtained from the digestive research are reasonable and logical. As it can be seen in Table 2, under all the same conditions, in metals and ceramics, with the increase of the coefficient of thermal expansion, the critical temperature difference decreases, so that the critical temperature difference in the cylinder made of alumina is more than that of silicon and that of nickel is more than that of stainless steel. and also, in general, in the same conditions, the critical temperature difference in ceramics is much higher than in metals, which can be considered one of the reasons for the high modulus of elasticity in these materials.

Next, the critical buckling load of the FGM shell under compressive loading is compared with the results of the

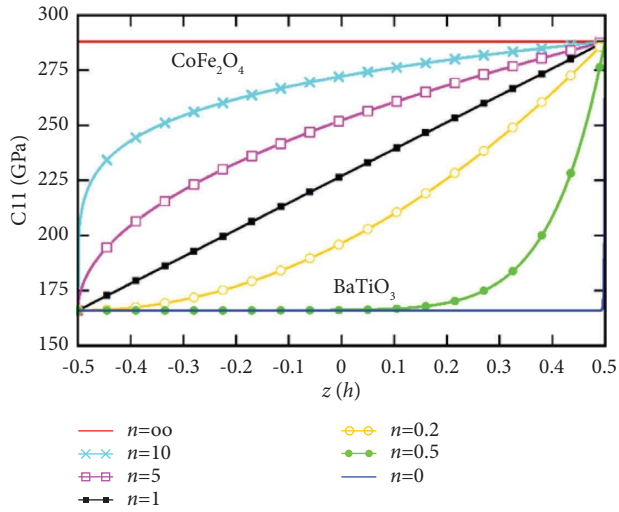

Figure 2: Changes in modulus of elasticity against thickness obtained from power changes in the power law relationship.

Table 2: Comparison of critical temperature distortion for an isotropic cylindrical shell for different materials.

Error	Reference results [3]	The results of the present method	h/R	Materials
0.07	256.8651	257.0345	0.008	Nickel
1.49	1564.4034	1604.7801	0.05	
0.51	221.3198	222.4519	0.008	Steel
0.44	1348.001	1353.9012	0.05	
1.47	460.3751	453.6189	0.008	Silicon Nitride
0.30	2771.0983	2762.8000	0.05	
1.93	458.1918	467.0391	0.008	Alumina
4.36	2790.6780	2912.3405	0.05	

studies conducted by Blooriyan et al. [4] and Bagherizadeh et al. [5] in Table 3.

The parameters used to extract the results of this table are as follows: From the comparison of the results of this research and the studies conducted by Blooriyan et al. [4] and Bagherizadeh et al. [5], they are compared in Table 3. The parameters used to derive the results of this table are as follows: $E_m = 70\,GPa$, $E_c = 380\,GPa$, and $\nu_m = \nu_c = 0.3$.

3.3. The Effect of Distribution of Properties in the Target Material. As a first step, the effect of the distribution of properties in the target material and boundary conditions on the critical buckling load of the FGMEE microshell was investigated, the results of which are presented in Tables 4 and 5. In Table 4, the critical mechanical force for different boundary conditions and for different values (L/R) and exponential distribution parameters of the properties are presented, and in Table 5, the critical temperature of microshell buckling with different boundary conditions is presented. The dimensions of the FGMEE microshell are considered as $h = 5\,\mu m$ and $(l/h) = 0.1$.

The boundary conditions of the beam are indicated by two English letters, where C is the symbol of braced support, S is simple support, and F is free support. For example, the CC represents the shell with bearing conditions on both its inner and outer edges, while the SS shell represents the shell with simple supports. The boundary condition of the shell is displayed with only one letter that indicates the type of support in the outer radius. As expected, the increase decreases the shell stiffness and thus the frequency. In addition, as can be seen, with the increase of n, the critical load of the shell increases, which was expected, because the increase of n causes an increase in the Young's modulus and, as a result, the bending stiffness of the structure.

Figure 3 shows the effect of the relative length parameter (L/R) on the buckling mechanical load of the FGMEE shell for different values of the material change exponent. As can be seen, the amount of buckling load decreases with the increase of the relative length. That is, the load bearing in shorter shells with larger n is more than long shells with lower n. In addition, as the profile of the target material increases, the critical load values also increase. Because with increasing the profile of the target material, the material is inclined towards the $CoFe_2O_4$ metal, as a result of which the modulus of elasticity increases, the material becomes harder, so the critical force increases. Similarly, by reducing the profile of the target material, the material is inclined towards the softer metal $BaTiO_3$ and the modulus of elasticity is reduced, thus the critical force is reduced. In addition, it can be seen that due to the presence of thermal loading in the

Table 3: Critical buckling load for FGM cylindrical shell under external compressive loading.

L/R	h/R					
	0.01			0.025		
	Present	Ref [4, 5]	Ref [4, 5]	Present	Ref [4, 5]	Ref [4, 5]
50	79.901	79.898	79.929	80.160	80.582	79.486
300	480.136	480.022	479.506	476.305	476.033	476.383
900	438.178	438.225	438.157	430.290	431.366	428.647

Table 4: Critical mechanical force of FGMEE shell for boundary conditions and different values and exponential distribution parameter.

BC	n	(L/R)			
		0.5	10	50	100
CC	0.2	0.78421	0.73012	0.64931	0.58013
	0.5	0.82369	0.68920	0.56178	0.46921
	1	0.98402	0.80341	0.63094	0.58902
SS	0.2	0.60342	0.45761	0.40349	0.20453
	0.5	0.76491	0.51739	0.48701	0.40983
	1	0.90385	0.62901	0.59351	0.44987

Table 5: Critical temperature of FGMEE shell for different boundary conditions and for different values and exponential distribution parameter.

BC	n	(L/R)			
		0.5	10	50	100
CC	0.2	753	725	680	620
	0.5	768	740	705	673
	1	782	759	731	708
SS	0.2	687	668	653	640
	0.5	702	689	670	658
	1	723	710	684	664

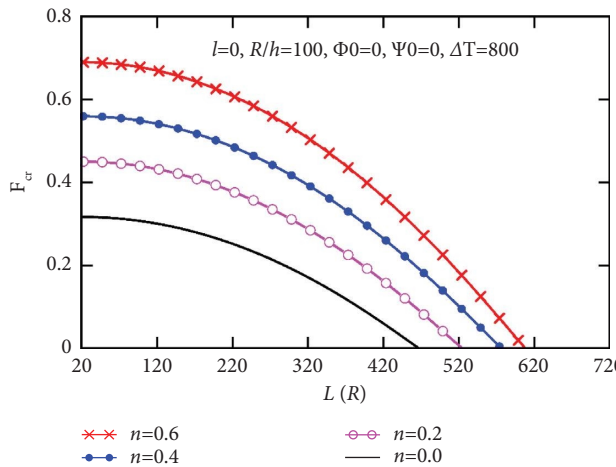

Figure 3: The effect of the relative length parameter (L/R) on the buckling mechanical load of the FGMEE shell for different values of the exponential power in the presence of a thermal field.

system, with the increase in the L/R ratio, the mechanical buckling force tends to zero, which is due to the presence of thermal compressive stresses in the structure, which cause thermal buckling in the FGMEE shell. For example, in the case of $L/R = 20$ for $n = 0$ and $n = 0.6$, the dimensionless critical buckling load of the system is equal to 0.32 and 0.68, respectively, which indicates an increase of 1.13 times in the shell buckling load. Figure 4 shows the effect of the relative

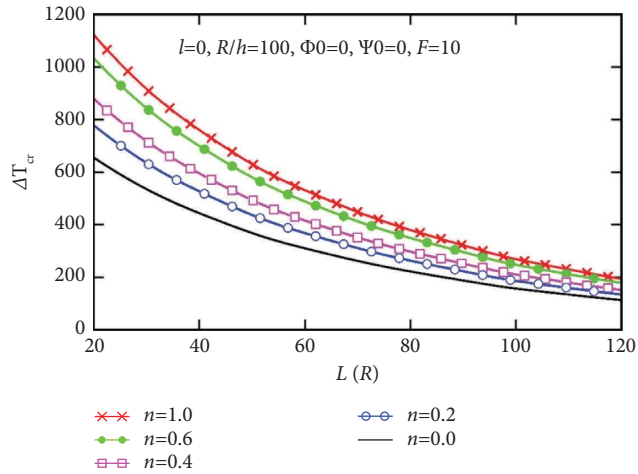

Figure 4: The effect of the relative length parameter (L/R) on the critical buckling temperature of the FGMEE shell for different values of the exponential power in the presence of a thermal field.

length parameter (L/R) on the critical buckling temperature of the FGMEE shell for different values of the material change exponent. As can be seen, with the increase of the length-to-radius ratio, the decreasing trend of the critical buckling temperature takes place at the beginning with a relatively large slope, but gradually, with the increase of the length-to-radius ratio, the slope of the changes decreases. Also, it can be seen that with the increase in the gradient index of the material, the critical buckling temperature of the shell increases, which is due to the increase in the equivalent stiffness of the structure as a result of the increase in the amount of $CoFe_2O_4$ solid material in the shell. It should be noted that according to Figure 4, in small L/R, the effect of the gradient index of the material on the critical temperature of buckling is greater and this effect decreases with the increase of the L/R ratio. For example, in the cases of $L/R = 20$ and $L/R = 120$, by increasing the gradient index of the material from 0 to 1, the critical temperature of the system increases by about 83% and 72%, respectively.

Figure 5 shows the effect of the material gradient index on the critical dimensionless axial buckling load. It has been shown that with the increase of the gradient index of the material, the critical buckling load becomes larger and tends to an asymptotic state for large values of n. The main reason for this increase can be stated as follows: for large amounts of n, the constituent material of the shell will be rich in $CoFe_2O_4$ components, which usually have more mechanical resistance than $BaTiO_3$ materials. Considering that the bending strength of the shell with $BaTiO_3$ metal is much less than that of the pure $CoFe_2O_4$ shell, as the volume percentage of $BaTiO_3$ material in the shell increases, the bending strength of the shell and, as a result, the critical axial buckling load decreases. With increasing the profile of the target material, the material tends towards the $CoFe_2O_4$ metal, and as a result, the modulus of elasticity increases and the stability of the structure increases. It is also observed that for smaller values of exponential power, the critical buckling load has more changes than for large values of n.

3.4. Effect of Electric Potential and Magnetic Potential. Magneto-electro-elastic materials show the internal coupling between magnetic, electric and elastic domains. Magneto-electro-elastic materials have common behavior between elastic, electric, and magnetic domains. These materials are not found in free form in nature, and in fact, the composite of a piezoelectric material and a piezomagnetic material forms the magneto-electro-elastic material. Magneto-electro-elastic materials release the strain caused by deformation in the form of electric and magnetic fields. With connecting electrodes to these materials and then connecting them to an electrical consumer, this mechanical energy can be converted into electromagnetic power. It should be mentioned that in order to convert the magnetic field into electric current, the magnetic field must first be converted into electric current using a coil or inductor. In general, smart materials can be used in all kinds of sensors and transducers due to their energy conversion properties. In particular, smart magneto-electro-elastic materials can be used as a source of power generation. with placing these materials in vibrating systems, their mechanical deformation can be extracted and stored as electrical power. Considering the increasing use of smart cylindrical microshells in microelectromechanical systems and ultra-sensitive sensors and ultra-fast actuators, the effect of various parameters on their mechanical performance is very important. Based on this, in this section, the effect of electric potential and magnetic potential on the critical buckling load and critical buckling temperature of the FGMEE microcylinder is studied. The effect of electric potential difference and magnetic potential intensity on the mechanical load of dimensionless buckling is shown in Figure 6. These results are presented for $L/R = 200$, $n = 0.4$ and $R/h = 100$ and in the presence of temperature field. According to Figure 6, it can be seen that the electric potential difference applied to the shell has a significant effect on the buckling load. From Figure 6, it can be seen that the positive electric potential difference causes the buckling load

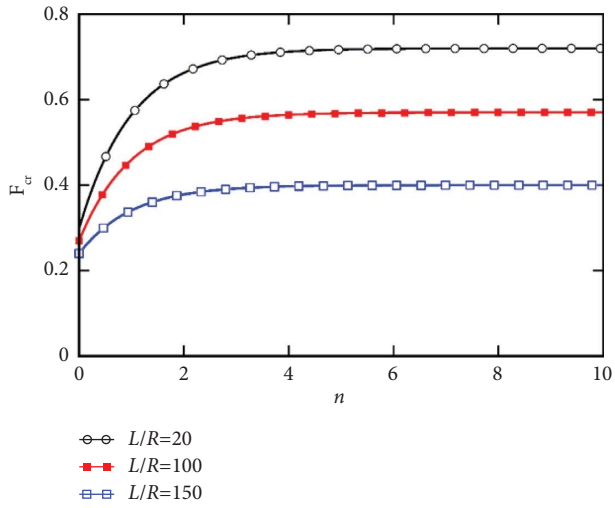

Figure 5: The effect of the material gradient index on the critical dimensionless axial buckling load of the FGMEE shell.

to decrease and the negative electric potential difference causes the shell buckling load to increase. Based on this, it can be said that the positive electric potential difference causes compressive stresses in the system and, accordingly, reduces the equivalent stiffness of the structure, and as a result, the shell buckles less due to external forces. The reverse of this behavior is true for a negative electric potential difference, and by applying a negative electric potential difference, tensile stresses are created in the structure, and as a result, the equivalent stiffness of the structure increases. As the stiffness of the structure increases, the tendency of the shell to change shape will decrease, and as a result, the bearing capacity of the FGMEE shell will increase. Based on the results, it can be seen that in the case of classical theory (for $l = 0$), applying the electric potential $\Phi 0 = 50\text{V}$ and $\Phi 0 = -50\text{V}$ difference to the magneto-electro-elastic shell causes a 43% decrease and a 42% increase in the critical buckling load of the system, respectively. Based on this, and according to the curve in Figure 6, it can be said that the effect of the electric potential difference on the changes in the buckling load of the structure is almost linear. These results are in acceptable agreement with the results presented by Liu et al. [6] for MEE nanosheets based on nonlocal theory. According to Figure 6, it can be seen that the critical buckling load of FGMEE microshell is affected by the magnetic potential and the effect of small sizes. The results show that the buckling load of the structure increases with the increase of the magnetic potential $\Psi 0$ due to the increase of the equivalent stiffness of the structure, and on the other hand, with the decrease of the magnetic potential and the increase of the small size parameter due to the softening effect of these parameters, the mechanical buckling load of the FGMEE cylindrical microshell decreases. It should be noted that, as can be seen, the increase in buckling load with increasing external magnetic potential and the decrease in buckling load with decreasing electric potential difference are both linear.

Table 6 shows the effect of magnetic potential and external electric potential on the critical buckling temperature of the FGMEE cylindrical microshell. These results are presented for $L/R = 200$, $n = 0.4$ and $R/h = 100$ in the presence of a temperature field. These results can be used as benchmark results to evaluate other numerical methods and also for the fast design of METE cylindrical shells in engineering applications. According to the results of this table, it can be seen that the effect of external electrical potential and also external mechanical potential on the critical buckling temperature of the system is similar to the external mechanical load. The critical buckling temperature of the FGMEE microshell decreases relatively linearly with increasing electric potential and increases with increasing magnetic potential. For $A\Psi = 0$ and $n = 0$, by increasing the external electric potential to 20 V and decreasing it to −20 V, the critical buckling temperature is obtained as 437.740 and 734.824, respectively, which indicates a 25% decrease and a 27% increase in the critical buckling temperature of the microshell is relative to the absence of external electric potential. In addition, the results show that the volume fraction of $BaTiO_3$ and $CoFe_2O_4$ materials in magneto-electro-elastic shells has a significant effect on the critical temperature. By increasing the gradient index of the material and increasing n, the amount of piezomagnetic cobalt ferrite material ($CoFe_2O_4$) in the FGMEE microshell increases, which increases the critical buckling temperature of the system.

According to the results of Figure 6, it can be concluded that the increase in the electric potential difference or the negative value of the external magnetic potential can cause the buckling of the FGMEE microshell. Considering that the increase in electric potential difference reduces the equivalent stiffness of the structure, buckling due to the increase in electric potential difference is logical. Based on this, in Figures 9 and 10, the effect of the gradient index of the material on the critical external electric potential as well as the critical external magnetic potential is shown. The results show that the increase in the gradient index of the material increases the magnetic potential and the critical electric potential, and the effect of the gradient index of the material

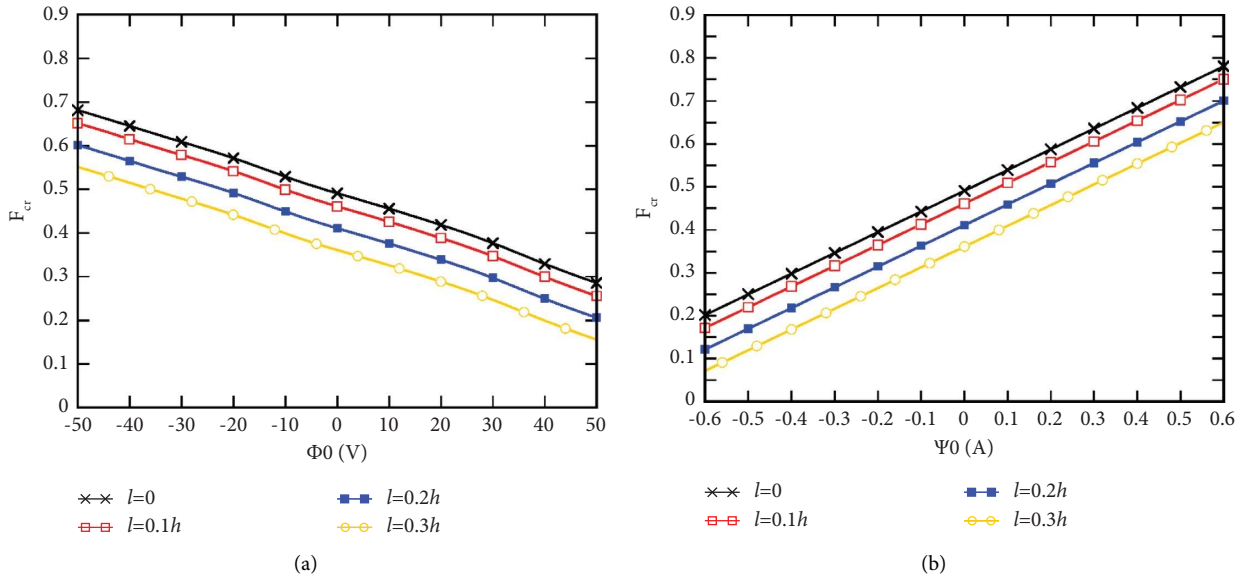

Figure 6: (a) Effect of electric potential difference and (b) magnetic potential on the mechanical load of dimensionless buckling of FGMEE cylindrical microshell for different values of small size parameter.

Table 6: The effect of external magnetic potential and electric potential on the critical buckling temperature of a FGMEE cylindrical microshell with boundary conditions of supporting supports at both ends.

Ψ0 (A)	Φ0 (V)				
	−20	−10	0	10	20
$n=0$					
−0.5	612.597	537.605	460.872	387.460	317.647
−0.2	672.659	596.847	521.454	448.286	369.879
0.0	734.824	659.008	583.875	544.345	477.740
0.2	795.946	725.170	632.457	569.534	492.342
0.5	857.143	789.331	648.877	631.765	557.973
$n=1$					
−0.5	884.313	806.501	730.688	654.876	579.063
−0.2	947.475	867.645	793.850	717.038	641.225
0	1008.64	935.838	859.034	779.199	703.386
0.2	1058.798	993.954	914.172	841.361	765.548
0.5	1135.959	1058.167	978.376	903.522	827.709

Note that it changes in a specific range, so the range of changes in external electric potential (Φ0) is greater than the range of changes in external magnetic potential (Ψ0). This is because the value is greater than and as a result of the results of the axial force and which are directly dependent on these constants, the effect of the force caused by the external electric potential will be less than the axial force caused by the external magnetic potential (Figures 7 and 8).

on increasing the critical magnetic potential is greater than its effect on the critical electric potential. For example, for $l/h=0$, with the increase of n from 0 to 4, the critical external electric potential and the critical external magnetic potential of the FGMEE microshell increase by about 22% and 82%, respectively. This phenomenon shows that external magnetic charges are also two effective factors in the structural stability of FGMEE cylindrical microshells. The volume fraction of the $BaTiO_3$ and $CoFe_2O_4$ phases and the external magneto-electric charges should be selected appropriately so that the performances of the FGMEE cylindrical microshell meet the requirements. In addition, it can be seen that the growth rate of the critical external magnetic potential with n is much higher than the corresponding case of the critical external electric potential, and for larger values of n, the effect of the functional graded distribution of materials on the critical values of the electric potential and magnetic potential almost converges to a certain value. In addition, the effect of the electric potential difference in increasing or decreasing the buckling load with effective properties close to piezoelectric is greater than its effect in increasing or decreasing its value with effective properties close to piezoelectric phase. It can be seen that when the gradient index of material n decreases, the critical buckling load decreases. The reason for this phenomenon is the reduction of the effective Young's modulus for magneto-electrostatic materials with an increase in the amount of piezoelectric material. Also, when a negative/positive electrical potential is applied to the system, tensile/compressive radial forces are generated that change the stiffness of the system and thus affect the

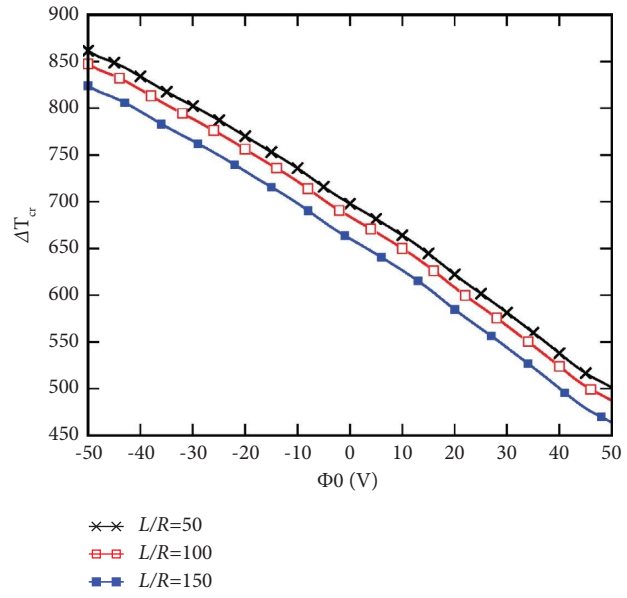

Figure 7: The effect of external electric potential on the critical buckling temperature difference ΔT_{cr} of the FGMEE microshell.

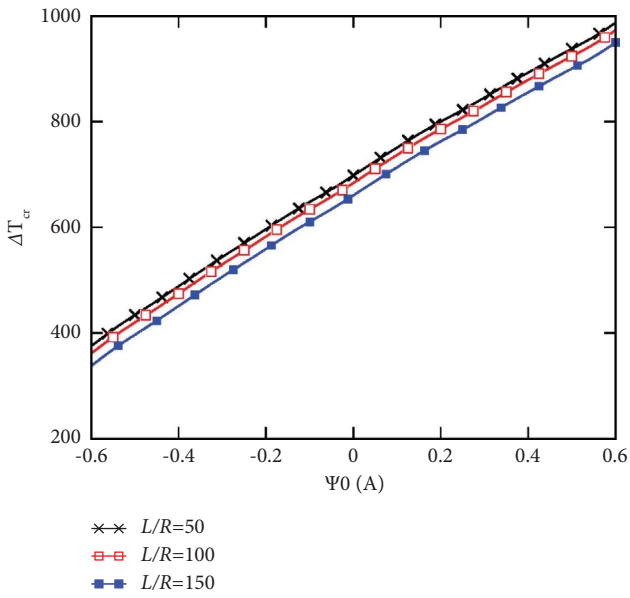

Figure 8: The effect of external magnetic potential on the critical buckling temperature difference ΔT_{cr} of the FGMEE microshell.

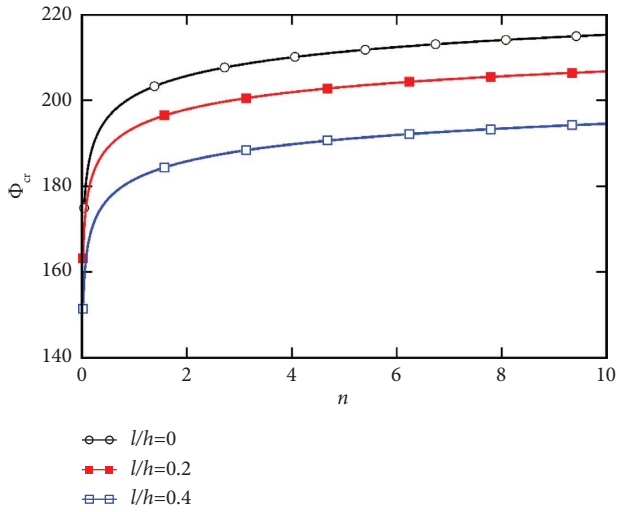

Figure 9: The effect of the material gradient index on the external critical electric potential of the FGMEE microshell.

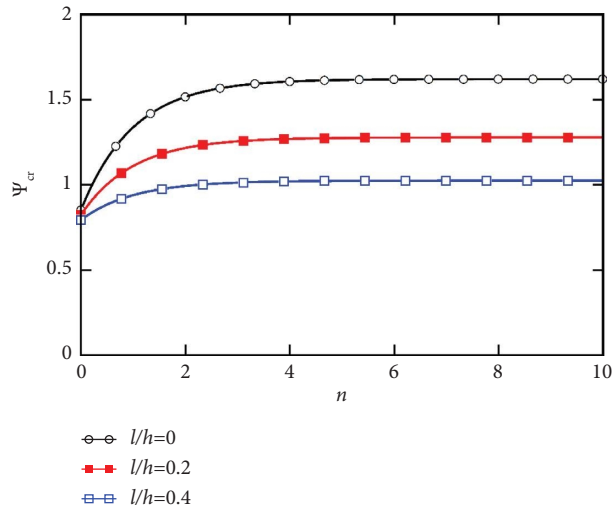

Figure 10: The effect of material gradient index on critical external magnetic potential of FGMEE microshell.

buckling load of the system. It should be noted that the greater the value of the positive magnetic potential, the higher the system stiffness and buckling load will be. In addition, the results shown in Figures 9 and 10 show that there is a significant difference between the length scale parameter in the buckling behavior of FGMEE microshells predicted by the modified Couple stress model and the classical model.

Considering that the thickness of FGMEE microshells also has a significant effect on the buckling behavior, therefore, the buckling load for different values of the h/R parameter, the small size parameter and the gradient index of the material are shown in Table 7. According to these results, it can be seen that the buckling load increases significantly with the increase of shell thickness; for example, with the increase of h/R from 0.01 to 0.5, the buckling load increases by about 4.8 times. Another result that can be seen according to Table 7 is that with the increase in the amount of $CoFe_2O_4$, its effect on increasing the buckling load decreases.

3.5. Thermal Buckling Analysis. In this article, the effect of various factors on the thermal buckling behavior of a magneto-electro-elastic microshell under combined mechanical and thermal loading is studied. Considering that in this research, three different types of heat transfer distribution in FMEE microshell are considered, which are:

Table 7: Buckling load of a functionally graded cylindrical magneto-electroelastic microshell by values of different parameters h/R, L/R, and exponential distribution.

n	h/R	$L/R = 40$		$L/R = 80$		$L/R = 150$		$L/R = 200$	
		$l/h = 0$	$l/h = 1$	$l/h = 0$	$l/h = 1$	$l/h = 0$	$l/h = 1$	$l/h = 0$	$l/h = 1$
0.00	0.01	0.45	0.34	0.42	0.31	0.38	0.29	0.31	0.26
	0.10	1.13	0.93	1.04	0.87	0.95	0.78	0.85	0.71
	0.20	1.44	1.32	1.33	1.11	1.21	1.02	1.20	1.00
	0.50	2.01	1.69	1.85	1.54	1.69	1.40	1.55	1.29
0.10	0.01	0.59	0.43	0.53	0.33	0.47	0.28	0.39	0.39
	0.10	1.27	1.07	1.31	1.01	1.17	0.91	0.97	0.88
	0.20	1.78	1.42	1.76	1.23	1.58	1.14	1.30	1.21
	0.50	2.67	2.14	2.65	1.95	2.39	1.69	1.96	1.96
0.30	0.01	0.79	0.54	0.66	0.44	0.60	0.32	0.49	0.43
	0.10	1.47	1.20	1.45	1.08	1.31	1.00	1.09	0.97
	0.20	2.04	1.62	2.00	1.42	1.80	1.24	1.48	1.28
	0.50	3.38	2.70	3.33	2.20	3.00	2.03	2.47	2.17
0.60	0.01	1.36	0.86	1.07	0.87	0.96	0.73	0.79	0.70
	0.10	2.30	1.80	2.23	1.81	2.01	1.64	1.65	1.45
	0.20	2.77	2.17	2.68	2.17	2.41	2.03	1.98	1.53
	0.50	4.56	3.62	4.48	3.63	4.03	3.39	3.31	3.01

(1) The temperature on the outer surface increases as much as $T\Delta$, and the temperature increases uniformly by the same amount throughout the entire thickness.

(2) The temperature on the outer surface increases as much as $T\Delta$ and remains constant on the inner surface of the cylinder at the ambient temperature, i.e., $T = 300$ K. In this case, the temperature changes from the outer surface to the inner surface are assumed to be linear.

(3) The temperature on the outer surface increases as much as $T\Delta$, and on the inner surface of the cylinder, it remains constant at the ambient temperature, i.e. $T = 300$ K, and the temperature changes follow the conduction law. Therefore, according to the relationships presented in the third chapter, the temperature change is assumed to be nonlinear.

Therefore, in this section, firstly, the effect of temperature distribution in the shell wall on the buckling of these shells is studied. Figure 11 shows the effect of heat transfer with uniform temperature distribution on buckling load of FGMEE microshell. In this figure, the effect of the ambient temperature on the mechanical buckling load is shown for different values of the gradient index of the material. According to this figure, it can be seen that, in general, with the increase in temperature and the gradient index of the material, the mechanical buckling load of FGMEE microshells increases significantly as a result of increasing the equivalent stiffness of the structure. For the FGMEE microshell for $n = 0.1$, the dimensionless mechanical buckling load at ambient temperature is equal to 0.3, and with the increase of temperature to 500 K, this value is equal to 0.15, which indicates a reduction of about 50% of the dimensionless critical mechanical buckling load. Also, for the cylindrical microshell for $n = 3$, the dimensionless buckling mechanical load at ambient temperature and 500 K temperature is equal to 1.27 and 0.88, respectively, which indicates a 31% decrease in the stability of the structure with increasing temperature. These results show that in the presence of piezomagnetic cobalt ferrite phase ($CoFe_2O_4$), the effect of temperature on the reduction of buckling load and instability of the structure is less.

Figure 12 shows the effect of heat transfer in a constant temperature state on the inner and outer surfaces of the shell and the linear temperature changes from the outer surface to the inner surface of the FGMEE shell on the buckling mechanical load. According to the results, it can be seen that this type of temperature distribution has a significant effect on reducing the buckling load of these types of shells, and as the temperature increases, the instability of the system occurs due to much less external forces. For example, for the microshell for $n = 0.1$, by increasing the temperature of the inner wall of the shell from 293 K to 500 K, the dimensionless buckling load of the system is about 0.35 and 0.10, respectively, which represents a 71% reduction in the mechanical buckling load. Also, similarly, it is observed that for the shell with the gradient index of the material equal to $n = 3$, the dimensionless buckling load of the system at the mentioned temperatures is about 2.4 and 0.93, respectively, which shows that the dimensionless buckling load is reduced by about 75%.

The effect of heat transfer in the case of nonlinear temperature change along the thickness on the buckling load of a double-walled FGMEE microshell is shown in Figure 13. As can be clearly seen, with the increase of the gradient index parameter of the material, the buckling load of the desired shell has increased and its hardness has increased. For example, at the ambient temperature of 293 K, with the increase of n from 0 to 3, the mechanical load of dimensionless buckling of the shell under investigation has increased by about 5.3 times.

In addition, another result is that according to the buckling load curves according to the temperature of the

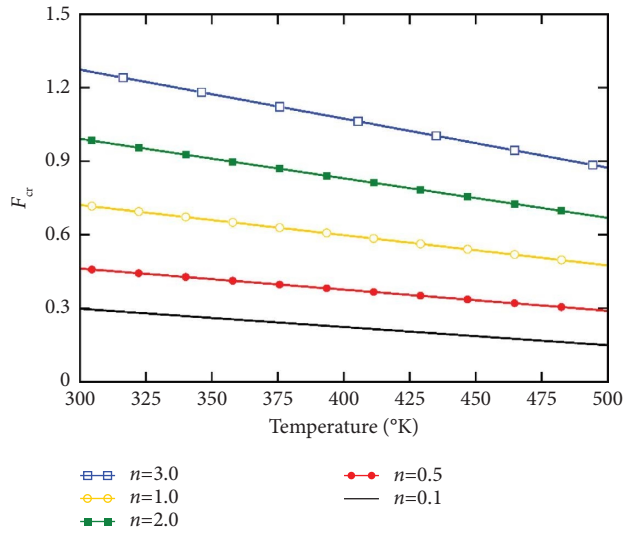

Figure 11: The effect of heat transfer with uniform temperature distribution on the buckling load of a double-walled magneto-electroelastic microshell.

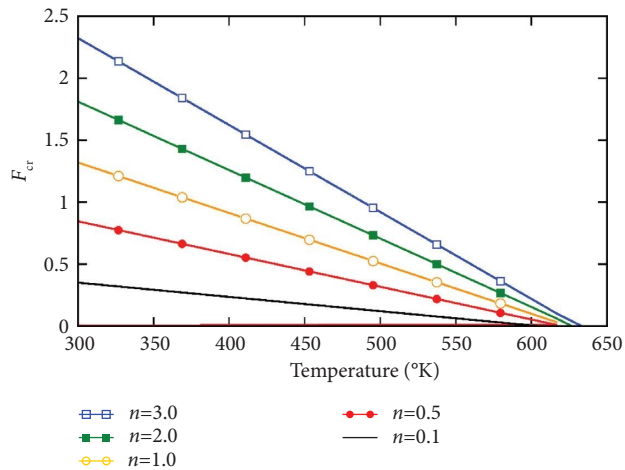

Figure 12: The effect of heat transfer in constant temperature state on the inner and outer surfaces and linear temperature changes from the outer surface to the inner surface of the shell on the buckling load of the magneto-electroelastic microshell per.

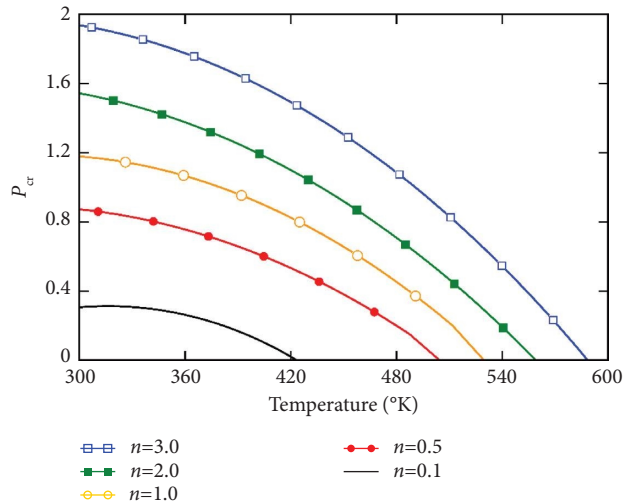

Figure 13: The effect of heat transfer in the case of constant temperature on the inner and outer surfaces of the shell and non-linear temperature changes from the outer surface to the inner surface of the shell on the buckling load of the magneto-electroelastic microshell per.

Table 8: Dimensionless critical buckling temperature of cylindrical magneto-electro-elastic microshell for different values of material gradient index and type of heat distribution in the shell wall.

How to distribute temperature	n	L/R			
		20	50	100	300
Uniform distribution	0.0		534.64		
	0.01	656.79	593.34	520.43	479.87
	0.1	736.15	686.91	617.02	528.98
Linear temperature distribution in the wall	0.0		508.22		
	0.01	585.37	554.37	547.34	516.79
	0.1	627.85	580.98	558.05	523.09
Nonlinear temperature distribution in the wall	0.0		407.08		
	0.01	414.42	403.82	388.07	372.73
	0.1	425.73	414.54	401.21	386.38

inner wall of the shell falls into three cases: uniform temperature distribution, temperature distribution assuming linearity along the thickness, and temperature distribution assuming nonlinearity along the thickness, as shown in Figures 11–13. As shown, it is observed that in cases of nonlinear temperature distribution in the shell wall and at high temperatures, thermal stresses have a significant effect on the dimensionless buckling load of the shell under investigation. As an example, for a shell with a material gradient index equal to 0.1 in three cases of uniform temperature distribution, linear temperature distribution in the wall and nonlinear temperature distribution in the wall of the FGMEE shell, the dimensionless buckling load at a temperature of 350 K is obtained as 0.26, 0.28, and 0.23, respectively. If at a temperature of 400 K, these values are equal to 0.22, 0.24, and 0.12, respectively. Meanwhile, with the increase in temperature from 350 K to 400 K, the drop in buckling capacity in three states of uniform temperature distribution, linear temperature distribution in the wall, and nonlinear temperature distribution in the wall of the FGMEE shell reaches 15%, 14%, and 47%, respectively. The reason for the greater drop in buckling capacity is caused by thermal stresses, and as a result, the equivalent stiffness of the structure decreases. According to Figures 4–12, it can be seen that for a certain value of the temperature difference between the inner and outer surfaces of the shell, the mechanical buckling load is equal to zero, and this corresponding temperature value is called the critical buckling temperature and by showing it, it will be given. In Table 8, the critical buckling temperature of the magneto-electro-elastic shell is shown for the gradient index values of the material and the type of heat distribution in the shell wall. According to the results of this table, it is clearly seen that the temperature distribution in the thickness of the shell has a significant effect on the critical buckling temperature of these shells. An interesting result that can be seen from the results of this table is that according to the way of temperature distribution in the shell wall, the critical buckling temperature is also obtained differently. For example, for the case of uniform temperature distribution in the shell wall, it is observed that by changing the heat distribution from uniform to linear and nonlinear, the critical temperature of shell buckling decreases. According to the results, the greater the degree of nonlinearity of heat distribution, the more significant the changes in the critical buckling load.

4. Conclusion

Based on these experiments, the main results are summarized as follows:

(i) With the increase of shell thickness, the buckling load increases significantly, and for example, with the increase of h/R from 0.01 to 0.5, the buckling load increases by about 4.8 times.

(ii) With increasing the amount of $CoFe_2O_4$ in magneto-electro-elastic cylindrical microshell materials, its effect on increasing the buckling load decreases.

(iii) Observed that in cases of nonlinear temperature distribution in the shell wall and at high temperatures, thermal stresses have a significant effect on the dimensionless buckling load of the shell under investigation.

(iv) For the shell with a material gradient index equal to 0.1 in three cases of uniform temperature distribution, linear temperature distribution in the wall, and nonlinear temperature distribution in the wall of the FGMEE shell, the dimensionless buckling load at 350 K is obtained as 0.26, 0.28, and 0.23 respectively; if at a temperature of 400 K, these values are equal to 0.22, 0.24, and 0.12, respectively.

(v) With the increase in temperature from 350 K to 400 K, the drop in buckling capacity in the three states of uniform temperature distribution, linear temperature distribution in the wall, and nonlinear temperature distribution in the wall of the FGMEE shell reaches 15%, 14%, and 47%, respectively. The reason for the greater drop in buckling capacity is caused by thermal stresses, and as a result, the equivalent stiffness of the structure decreases.

(vi) For the case of uniform temperature distribution in the shell wall, it is observed that the critical temperature of shell buckling decreases with the change of heat distribution from uniform to linear and non-linear. According to the results, the greater the degree of non-linearity of heat distribution, the more significant the changes in the critical buckling load.

(vii) The buckling force of the FGMEE microshell decreases with the increase of the small size parameter, which is due to the softening effect of the small size parameter on the equivalent stiffness of the structure.

(viii) For FGMEE microshell, buckling load decreases linearly with increasing electric potential and increases with increasing magnetic potential.

(ix) In the case of classical theory (for $l = 0$), applying the electric potential difference to the magneto-electroelastic shell causes a 43% decrease and a 42% increase in the critical buckling load of the system, respectively.

(x) The effect of the electric potential difference on the buckling load changes of the structure is almost linear.

(xi) The buckling load of the structure increases with the increase of the magnetic potential due to the increase of the equivalent stiffness of the structure, and on the other hand, with the decrease of the magnetic potential and the increase of the small size parameter due to the softening effect of these parameters, the mechanical buckling load of the FGMEE cylindrical microshell decreases.

(xii) It should be noted that, as can be seen, the increase in buckling load with increasing external magnetic potential and also, the decrease in buckling load with decreasing electric potential difference is linear.

(xiii) For $A\Psi = 0$ and $n = 0$, by increasing the external electric potential to 20 V and decreasing it to -20 V, the critical buckling temperature is obtained as 437.740 and 734.824 respectively, which shows a 25% decrease and a 27% increase. At the critical buckling temperature of the microshell, it is relative to the absence of external electric potential.

(xiv) The volume fraction of $BaTiO_3$ and $CoFe_2O_4$ materials in magneto-electro-elastic shells has a significant effect on the critical temperature. By increasing the gradient index of the material and increasing n, the amount of piezomagnetic cobalt ferrite material ($CoFe_2O_4$) in the FGMEE microshell increases and this increases the critical buckling temperature of the system.

Conflicts of Interest

The authors declare that they have no conflicts of interest.

References

[1] A. Shooshtari and S. Razavi, "Linear and nonlinear free vibration of a multilayered magneto-electro-elastic doubly-curved shell on elastic foundation," *Composites Part B: Engineering*, vol. 78, pp. 95–108, 2015.

[2] P. Seide, "Axisymmetrical buckling of circular cones under axial compression," *Industrial Chocolate Manufacture and Use*, vol. 56, no. 2, pp. 56–78, 1956.

[3] F. Moradi and M. S. Jafari, "Magneto-thermo-elastic buckling analysis of 2D-FGM open cylindrical shell by GDQ method," *Journal of Alloys and Compounds*, vol. 124, no. 5, pp. 66–90, 2017.

[4] S. Blooriyan, R. Ansari, A. Darvizeh, R. Gholami, and H. Rouhi, "Postbuckling analysis of functionally graded graphene platelet-reinforced polymer composite cylindrical shells using an analytical solution approach," *Applied Mathematics and Mechanics*, vol. 40, no. 7, pp. 1001–1016, 2019.

[5] E. Bagherizadeh, Y. Kiani, and M. Eslami, "Mechanical buckling of functionally graded material cylindrical shells surrounded by Pasternak elastic foundation," *Composite Structures*, vol. 93, no. 11, pp. 3063–3071, 2011.

[6] C. Liu, L. L. Ke, Y. S. Wang, J. Yang, and S. Kitipornchai, "Thermo-electro-mechanical vibration of piezoelectric nanoplates based on the nonlocal theory," *Composite Structures*, vol. 106, pp. 167–174, 2013.

[7] D. J. Leo, *Engineering Analysis of Smart Material Systems*, John Wiley and Sons, New York, NY, USA, 2007.

[8] D. M. Addington and D. L. Schodek, *Smart Materials and New Technologies: For the Architecture and Design Professions*, Routledge, Oxfordshire, England, UK, 2005.

[9] J. Van Suchtelen, "Product properties: a new application of composite materials," *Philips Research Reports*, vol. 27, no. 1, pp. 28–37, 1972.

[10] J. Boomgaard, D. R. Terrell, R. A. J. Born, and H. F. J. I. Giller, "An in situ grown eutectic magnetoelectric composite material," *Journal of Materials Science*, vol. 9, no. 10, pp. 1705–1709, 1974.

[11] P. C. Y. Lee, "A variational principle for the equations of piezoelectromagnetism in elastic dielectric crystals," *Journal of Applied Physics*, vol. 69, no. 11, pp. 7470–7473, 1991.

[12] J. Y. Li and M. L. Dunn, "Micromechanics of magneto-electroelastic composite materials: average fields and effective behavior," *Journal of Intelligent Material Systems and Structures*, vol. 9, no. 6, pp. 404–416, 1998.

[13] G. R. Buchanan, "Layered versus multiphase magneto-electro-elastic composites," *Composites Part B: Engineering*, vol. 35, no. 5, pp. 413–420, 2004.

[14] C.-W. Nan, M. I. Bichurin, S. Dong, D. Viehland, and G. Srinivasan, "Multiferroic magnetoelectric composites: historical perspective, status, and future directions," *Journal of Applied Physics*, vol. 103, no. 3, p. 031101, 2008.

[15] A. Yousefi-Koma and D. G. Zimcik, "Applications of smart structures to aircraft for performance enhancement," *Canadian Aeronautics and Space Journal*, vol. 49, no. 4, pp. 163–172, 2003.

[16] J. Valente, J.-Y. Ou, E. Plum, I. J. Youngs, and N. I. Zheludev, "A magneto-electro-optical effect in a plasmonic nanowire material," *Nature Communications*, vol. 6, no. 1, pp. 7021–7027, 2015.

[17] P. Franciosi, "Transversally isotropic Magneto-Electro-Elastic composites with co-(dis) continuous phases," *International*

Journal of Solids and Structures, vol. 50, no. 6, pp. 1013–1031, 2013.

[18] Z. Zhang and X. Wang, "Effective multi-field properties of electro-magneto-thermoelastic composites estimated by finite element method approach," *Acta Mechanica Solida Sinica*, vol. 28, no. 2, pp. 145–155, 2015.

[19] J. Lee, J. G. Boyd, and D. C. Lagoudas, "Effective properties of three-phase electro-magneto-elastic composites," *International Journal of Engineering Science*, vol. 43, no. 10, pp. 790–825, 2005.

[20] I. A. Starkov and A. S. Starkov, "Effective parameters of multilayered thermo-electro-magneto-elastic solids," *Solid State Communications*, vol. 226, pp. 5–7, 2016.

[21] M. Vinyas and S. C. Kattimani, "A finite element based assessment of static behavior of multiphase magneto-electro-elastic beams under different thermal loading," *Structural Engineering & Mechanics*, vol. 62, no. 5, pp. 519–535, 2017.

[22] M. Vinyas, S. C. Kattimani, and S. Joladarashi, "Hygrothermal coupling analysis of magneto-electroelastic beams using finite element methods," *Journal of Thermal Stresses*, vol. 41, no. 8, pp. 1063–1079, 2018.

[23] A. Alaimo, I. Benedetti, and A. Milazzo, "A finite element formulation for large deflection of multilayered magneto-electro-elastic plates," *Composite Structures*, vol. 107, pp. 643–653, 2014.

[24] A. Milazzo, "Large deflection of magneto-electro-elastic laminated plates," *Applied Mathematical Modelling*, vol. 38, no. 5–6, pp. 1737–1752, 2014.

[25] C. X. Xue, E. Pan, S. Y. Zhang, and H. J. Chu, "Large deflection of a rectangular magnetoelectroelastic thin plate," *Mechanics Research Communications*, vol. 38, no. 7, pp. 518–523, 2011.

[26] M. F. Liu, "An exact deformation analysis for the magneto-electro-elastic fiber-reinforced thin plate," *Applied Mathematical Modelling*, vol. 35, no. 5, pp. 2443–2461, 2011.

[27] H.-Y. Kuo and E. Pan, "Effective magnetoelectric effect in multicoated circular fibrous multiferroic composites," *Journal of Applied Physics*, vol. 109, no. 10, Article ID 104901, 2011.

[28] P. L. Bishay, J. Sladek, V. Sladek, and S. N. Atluri, "Analysis of functionally graded magneto-electro-elastic composites using hybrid/mixed finite elements and node-wise material properties," *Computers, Materials & Continua*, vol. 29, no. 3, p. 213, 2012.

[29] C.-C. Ma and J.-M. Lee, "Theoretical analysis of in-plane problem in functionally graded nonhomogeneous magneto-electroelastic bimaterials," *International Journal of Solids and Structures*, vol. 46, no. 24, pp. 4208–4220, 2009.

[30] T. M. Badri and H. H. Al-Kayiem, "Analytical solution for simply supported and multilayered magneto-thermo-electro-elastic plates," *Asian journal of scientific research*, vol. 6, no. 2, pp. 236–244, 2012.

[31] A. H. Akbarzadeh and Z. T. Chen, "Magnetoelectroelastic behavior of rotating cylinders resting on an elastic foundation under hygrothermal loading," *Smart Materials and Structures*, vol. 21, no. 12, Article ID 125013, 2012.

[32] J. Kim and A. Baltazar, "Pyroelectric and Pyromagnetic Coefficients of Functionally Graded Multilayered Multiferroic Composites," *Acta Mechanica*, vol. 223, no. 4, pp. 849–860, 2012.

[33] M. Arefi, "A complete set of equations for piezo-magnetoelastic analysis of a functionally graded thick shell of revolution," *Latin American Journal of Solids and Structures*, vol. 11, no. 11, pp. 2073–2092, 2014.

[34] C.-P. Wu and Y.-C. Lu, "A modified Pagano method for the 3D dynamic responses of functionally graded magneto-electro-elastic plates," *Composite Structures*, vol. 90, no. 3, pp. 363–372, 2009.

[35] S. S. Phoenix, S. K. Satsangi, and B. N. Singh, "Layer-wise modelling of magneto-electro-elastic plates," *Journal of Sound and Vibration*, vol. 324, no. 3–5, pp. 798–815, 2009.

[36] Y. Ootao and M. Ishihara, "Transient thermal stress problem of a functionally graded magneto-electro-thermoelastic hollow cylinder due to a uniform surface heating," *Journal of Thermal Stresses*, vol. 35, no. 6, pp. 517–533, 2012.

[37] J. Sladek, V. Sladek, S. Krahulec, C. S. Chen, and D. L. Young, "Analyses of circular magnetoelectroelastic plates with functionally graded material properties," *Mechanics of Advanced Materials and Structures*, vol. 22, no. 6, pp. 479–489, 2015.

[38] D. J. Huang, H. J. Ding, and W. Q. Chen, "Static analysis of anisotropic functionally graded magneto-electro-elastic beams subjected to arbitrary loading," *European Journal of Mechanics - A: Solids*, vol. 29, no. 3, pp. 356–369, 2010.